



Calculation and Measurement of the Magnetic Field of Nd₂Fe₁₄B Magnets for High-Temperature Superconducting Magnetic Bearing Rotor

Yincai Zou^{1,2} · Xing Bian¹ · Jin Shang^{1,2} · Xiang Guan^{1,2} · Jihao Wu^{1,2} · Qing Li^{1,2}

Received: 8 May 2019 / Accepted: 11 September 2019 / Published online: 17 October 2019
© Springer Science+Business Media, LLC, part of Springer Nature 2019

Abstract

The external magnetic flux density and distribution of the permanent magnet (PM) rotor of the high-temperature superconducting (HTS) magnetic bearing directly affect the load-carrying properties and stability of the HTS magnetic bearing. In order to facilitate the design of the PM rotor that meets the application requirements, a finite element analysis (FEA) method to calculate the magnetic flux density and distribution of PM rings and PM rotor would be used. A magnetic field measurement system was built as well. By comparing the results of calculation and measurement, the validity of the magnetic field calculation method is verified. And the calculation results are promoted after correcting the calculation parameters of the magnetic ring. Therefore, the correctness and accuracy of the calculation method are verified by experimental measurement. The magnetic field measurement system can be used to measure and select the magnetic rings with uniform and consistent magnetic field to improve the stability of the HTS magnetic bearing. And the performance of the Nd₂Fe₁₄B magnets N52 at liquid nitrogen temperature (77 K) was measured, which has been increased by about 9% relative to magnetic field at room temperature (295 K).

Keywords High-temperature superconducting magnetic bearing · Nd₂Fe₁₄B magnets · Magnetic field calculation method · Experimental measurement

1 Introduction

In the large-scale superfluid helium cryogenic refrigeration system, the helium cold compressor is the key equipment for obtaining superfluid, and its operating conditions have the characteristics of low temperature and high speed [1, 2]. Radial high-temperature superconducting (HTS) magnetic bearings are suitable for high-speed rotating machinery [3–6]. The suspension performance and high-speed rotation stability of HTS magnetic bearings directly affect their application in helium cold compressor.

Due to the Nd-Fe-B, permanent magnets have advantages such as high coercivity, high magnetic energy product and remanence, as well as, they have been used in electric,

medical, electrical and electronic, energy, transportation, and other fields successfully [7–10]. Thus, it is a simple, lightweight, high-efficiency, and energy-saving way [11] for HTS magnetic bearings use Nd-Fe-B permanent magnet (PM) rotors to provide external magnetic fields.

However, the performance of HTS magnetic bearings highly depends on the magnetic flux density and distribution of PM rotors [12], the rotors need to be designed properly so that the magnetic flux and distribution can meet the application requirements. In order to facilitate the design of HTS magnetic bearing rotor, it is necessary to find a suitable way to calculate the magnetic field of the permanent magnets and PM rotor. In addition, the uniformity of the circumferential magnetic field of the PM rotor will affect the rotational loss and rotational stability of the HTS magnetic bearing. The performance of the permanent magnets at low temperatures will affect the application of the HTS magnetic bearing.

In this paper, the magnetic field calculation of permanent magnets was carried out by using ANSYS finite element analysis (FEA) software, and the calculation results of magnetic flux density and distribution of permanent magnets and PM rotors are obtained. Besides, a magnetic field measurement

✉ Qing Li
liqing@mail.ipc.ac.cn

¹ State Key laboratory of Technologies in Space Cryogenic Propellants, Technical Institute of Physics and Chemistry, Chinese Academy of Sciences, Beijing 100190, China

² University of Chinese Academy of Sciences, Beijing 100049, China

system was built to verify the correctness and accuracy of the finite element method and to measure the uniformity of the magnetic field of the magnetic rings and the performance of the $\text{Nd}_2\text{Fe}_{14}\text{B}$ magnets N52 at liquid nitrogen temperature (77 K).

2 Methods

2.1 Rotor Geometry

For the radial high-temperature superconducting magnetic bearing used in the centrifugal compressor, it is mainly composed of a superconducting stator and a permanent magnet (PM) rotor. The superconducting stator is composed of superconductors. The PM rotor is composed of stacked PM rings and iron rings, and the magnetic poles of adjacent end faces of PM rings are the same (···N SS NN SS NN S···). The PM ring magnetic field is concentrated and redistributed in the iron ring. The PM rotor is assembled on the shaft to form a bearing rotor. Figure 1 is a schematic structural diagram of a radial-type HTS magnetic bearing.

The force exerted by a permanent magnet on a superconductor is given by the gradient of the volume integral $F = -\text{grad} \int (M \times B) dV$, where B is the magnetic flux density produced by the PM configuration, and M is magnetization of the superconductor [13].

As the excitation source of HTS magnetic bearing, the PM rotor directly affects its magnetic flux density and spatial magnetic flux distribution, which has an important impact on the performance of HTS magnetic bearing. Finding a correct and accurate method for calculating the magnetic field of PM rotor can facilitate the structure design of PM rotor for helium cold compressor application and can save costs. In this study, a

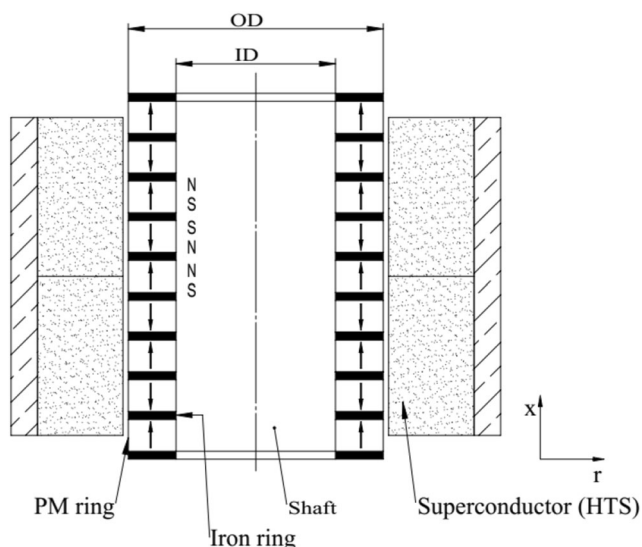


Fig. 1 Schematic structure diagram of HTS bearing

rotor of HTS magnetic bearing has been designed and manufactured, as shown in Fig. 2. The total length of the PM rotor is 70 mm, the inner diameter (ID) is 30 mm, and the outer diameter (OD) is 48 mm. The PM rotor includes eight PM rings with a thickness of 5.6 mm and two end PM rings with a thickness of 2.8 mm. The material of the PM rings is $\text{Nd}_2\text{Fe}_{14}\text{B}$ (N52).

2.2 Finite Element Analysis of Magnetic Field

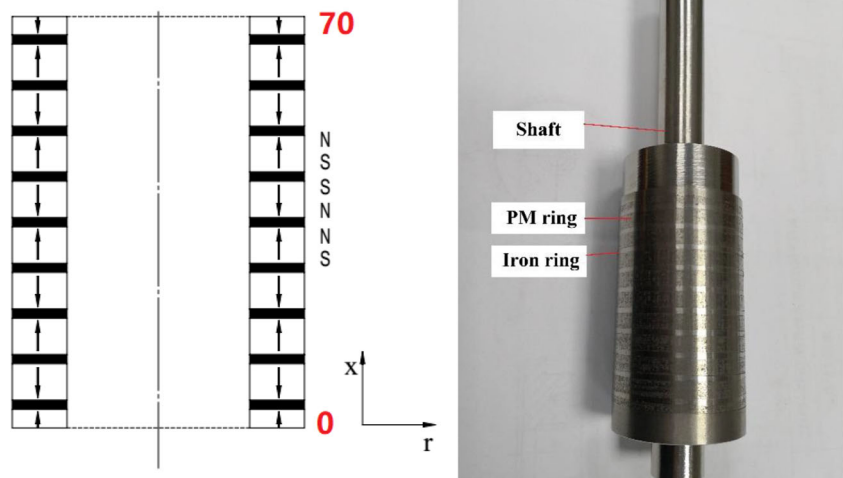
In this study, ANSYS finite element simulation software was used to calculate the magnetic flux density and distribution of magnets. First, building the computational modal which includes the geometry and the spatial enclosure cushion domain surrounded by the geometry. Second, defining the material properties. The permanent magnets ($\text{Nd}_2\text{Fe}_{14}\text{B}$) are defined as linear “hard” magnetic material by coercive force and residual induction, the iron rings (Silicon core iron) are defined as non-linear “soft” magnetic material by B-H curve, and the enclosure cushion domain (air) is defined as linear “soft” magnetic material by isotropic relative permeability. Third, defining the orientation direction of the permanent magnets. The magnetic rings are axially magnetized. The orientation direction of PM rings is parallel to the X axis. Fourth, meshing the computational modal. Finally, getting solution and results extraction.

Before the finite element analysis and experimental measurement of the PM rotor, the comparison research of FEA calculation and experimental measurement of a single PM ring were carried out, which can obtain the magnetic flux density and distribution results of the magnetic ring and verify the correctness and accuracy of the finite element calculation method. Next, the finite element calculation process is further studied based on the calculation model of a single PM ring.

Figure 3 is the geometry model of a single PM ring used to form a bearing rotor, the inner diameter (r) is 30 mm, the outer diameter (R) is 48 mm, the axis thickness (L) is 5.6 mm (r 30 mm \times R 48 mm \times L 5.6 mm). The spatial enclosure cushion domain is a cylinder that is coaxial with the ring. The initial residual induction is 1.434 T and the coercive force is 945 kA/m.

The distance from the outer surface of the PM ring geometry to the outer surface of the enclosure cushion domain will affect the calculation results. The larger the enclosure cushion distance is, the smaller the influence on the magnetic field calculation results is, but at the same time, it will occupy more computing resources, so, it is necessary to find the appropriate enclosure cushion distance. The calculation of the influence of the enclosure cushion distance on the magnetic field of the magnetic ring was carried out. Figure 4 declares the calculation results about the maximum value of magnetic flux density B and the enclosure cushion distance. The calculated value is taken from the path of $-40 \text{ mm} \leq Z \leq 40 \text{ mm}$, $X = 6.6 \text{ mm}$,

Fig. 2 HTS magnetic bearing rotor: PM rotor structure (left); photo of rotor (right)



$Y=0$ mm, which is 1 mm from the surface of the PM ring (designed gap of HTS magnetic bearing stator and rotor is 1 mm). It can be seen that when the enclosure cushion distance of the calculation model is 55 mm, it will not affect the calculation results and save computing resources.

In order to improve the accuracy of the calculation results, and avoid taking up too much computing resources and time, grid independence verification is required before performing the subsequent calculation. As shown in Fig. 5, when the number of mesh nodes reaches about 10^6 , the maximum value of magnetic flux density B on the path of $-40 \text{ mm} \leq Z \leq 40 \text{ mm}$, $X=6.6 \text{ mm}$, $Y=0 \text{ mm}$, almost no longer changes with the grid number, so it is reasonable and meaningless to continually increase the number of grids.

2.3 Magnetic Field Measurement System

In order to verify the correctness and accuracy of the calculation results, a magnetic field measurement system was designed and built.

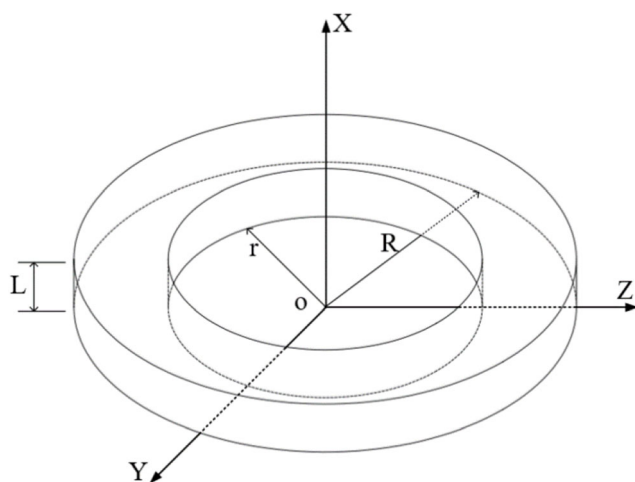


Fig. 3 Magnetic ring calculation model

The composition of the magnetic field measurement system is shown in Fig. 6. It mainly includes probe support and clamping mechanism 1, electronically controlled moving mechanism 1, electronically controlled moving mechanism 2, sample stage 3, and control collection analysis system 4.

The probe support and clamping mechanism 1 designed for this magnetic field measurement system can adjust the position of probe in two mutually perpendicular directions as well as the degrees of probe in two mutually perpendicular planes. It is available to orientate within a wide and full range.

The electronically controlled moving mechanism 2 is connected with the probe support and clamping mechanism, which includes X axis moving mechanism, Y axis moving mechanism, Z axis moving mechanism, and rotating moving mechanism. During the precision moving experiment, the electronically controlled moving mechanism drives the probe support and clamping mechanism to locate precisely on the X , Y , and Z axis directions. The rotating moving mechanism 14 is a rotation tester which aims at the magnetic field measurement setting with rotating symmetry axis. In order to facilitate the

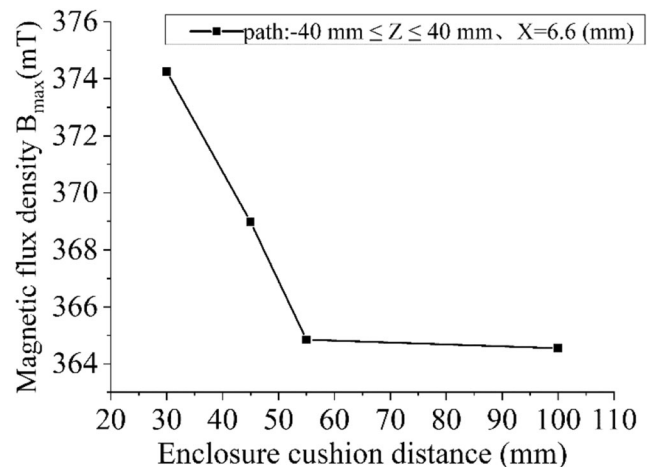


Fig. 4 Magnetic flux density versus enclosure cushion distance

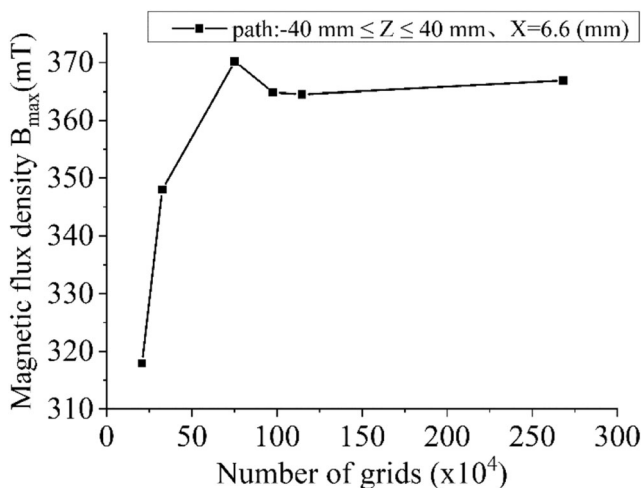


Fig. 5 Grid-independent verification

measurement of the magnetic field in space, the tested sample table should be placed on the rotating moving mechanism 14.

The sample stage 3 comprises a non-magnetic cushion and a sample table. The sample table includes the measured magnet and magnet holder, and the magnet holder is non-magnetic material. For the measured magnet with rotational axis of symmetry, the sample stage adopts a cylindrical structure to facilitate the adjustment of the concentric degree of the measured magnet and the rotating moving mechanism.

The control collection analysis system 4 includes industrial personal computer (IPC), motor drive controller 5, and gauss meter 6.

The IPC contains a system software to control the drive of motor and data acquisition and processing of gauss meter. It includes a drive control module, a serial communication module, a signal conversion module, a data storage module, a data processing module, and a display output module. The driver control program of the motor drive controller exists in the drive control module.

Gauss meter has the function of amplifying the voltage signal of the hall sensor and the A/D conversion and data

processing and display. The data collected by gauss meter can be stored, image drawn, exported, and displayed by connecting IPC and serial communication. The gauss meter of one-dimensional channel can be connected with a hall sensor, and the gauss meter of three-dimensional channel can be connected with three hall sensors. It is convenient to get the magnetic flux density B_x , B_y , and B_z in X , Y , and Z axes when three hall sensors are distributed on these three axes. The vector sum B is obtained by formula

$$= \sqrt{(B_x)^2 + (B_y)^2 + (B_z)^2}.$$

Figure 7 is the photo of magnetic field measurement system.

The main technical parameters of the measurement system are as follows:

1. The repositioning precision of the X , Y , and Z axes of the electronically controlled mobile mechanism is 0.01 mm, and the resolution of the rotating mobile mechanism is 0.0002°.
2. Gauss meter has a range of 30 T, and a resolution of 1 mG. It has temperature compensation function and its DC measurement precision error is within ± 0.15% of the reading. The diameter of three-dimensional probe is 3 mm. The thickness and width of one-dimensional cryogenic probe are 0.6 mm and 2.2 mm separately. It can be used at liquid nitrogen temperature (77 K), and the DC measurement precision is within ± 0.05% (0–2 T) of the reading.

3 Experiment

For Nd₂Fe₁₄B magnets N52, the magnetic flux density and spatial magnetic flux distribution on the surface space path (–40 mm < Z < 40 mm) of the PM ring (r 30 mm × R 48 mm × L

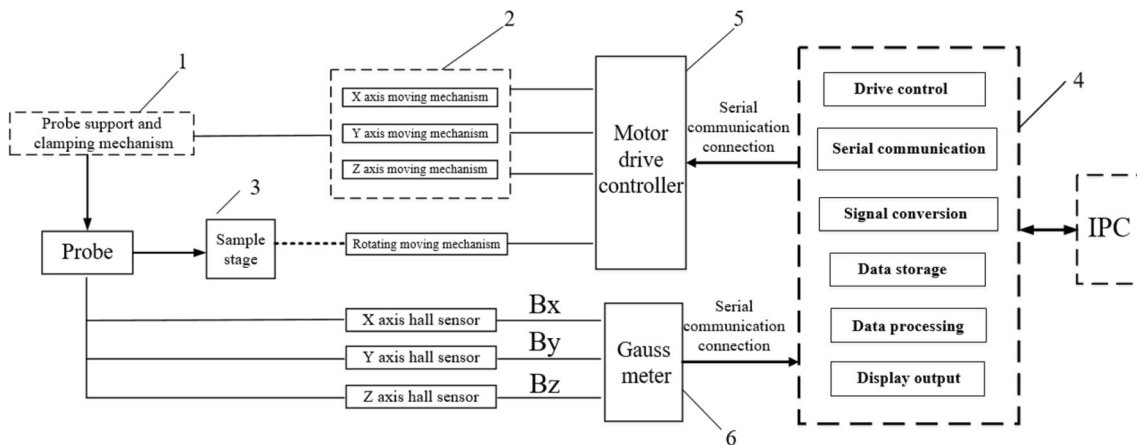
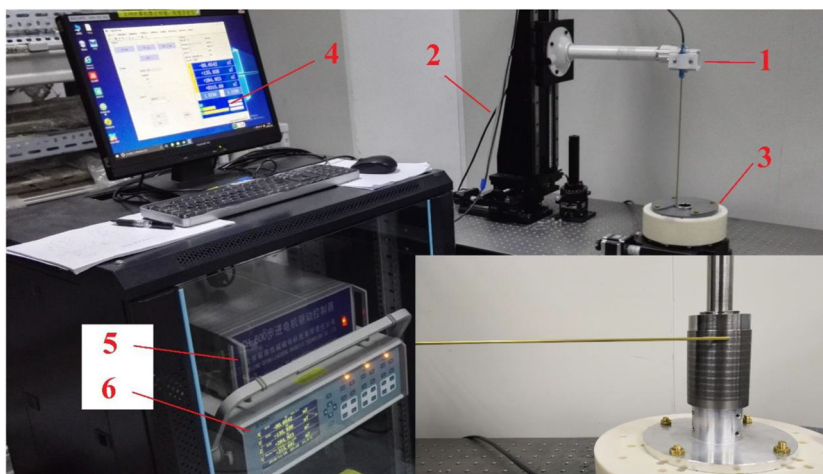


Fig. 6 Magnetic field measurement system composition diagram

Fig. 7 Photo of magnetic field measurement system: rotor measurement (lower right corner). 1—probe support and clamping mechanism, 2—electronically controlled moving mechanism, 3—sample stage, 4—control collection analysis system, 5—drive controller, 6—gauss meter



5.6 mm) as shown in Fig. 3 were measured, and the magnetic field on the path ($-15 \text{ mm} < X < 85 \text{ mm}$) of the PM rotor (ID $30 \text{ mm} \times \text{OD } 48 \text{ mm} \times 70 \text{ mm}$) as shown in Fig. 2 was measured. In addition, the uniformity measurement of circumferential magnetic field of the PM rings and the magnetic field measurement of the PM rings at the liquid nitrogen temperature (77 K) were carried out.

4 Results and Discussion

4.1 Calculated and Measured Results of Magnetic Ring Magnetic Field

Since the magnetic flux density of the permanent magnet decays obviously in space, in order to get large levitation force and high levitation stiffness, the permanent magnets should be placed as closely as possible to the nearby superconductors. The gap of the designed HTS magnetic bearing stator and rotor in this study is 1 mm; therefore, this paper mainly analyzes the magnetic field at a distance of 1 mm from the surface of the permanent magnet. The calculated value and measured value of the magnetic field B_x , B_y , B_z , and vector sum B on the path of $-40 \text{ mm} \leq Z \leq 40 \text{ mm}$, $X = 6.6 \text{ mm}$, $Y = 0 \text{ mm}$, are shown in Fig. 8.

From a, c, and d of Fig. 8, it can be seen that the calculation results are generally consistent with the trend of the measurement results, but the measured value is smaller than the calculated value. It can be seen from Fig. 8b that both the calculated value and the measured values, which should be zero due to the symmetric shape of the magnet, are not zero. The reason is the measurement path of Y axis hall sensor is not parallel to the hall sensor surface and does not pass through the geometric center of the magnetic ring. Considering that the measured value and calculated value of B_y are too small with respect to its vector sum B value, it is accepted.

In conclusion, the magnetic field calculation results are consistent with the measurement results, only the numerical values are slightly inaccurate. Consequently, it is reasonable to use the method to calculate the magnetic flux distribution of magnetic ring.

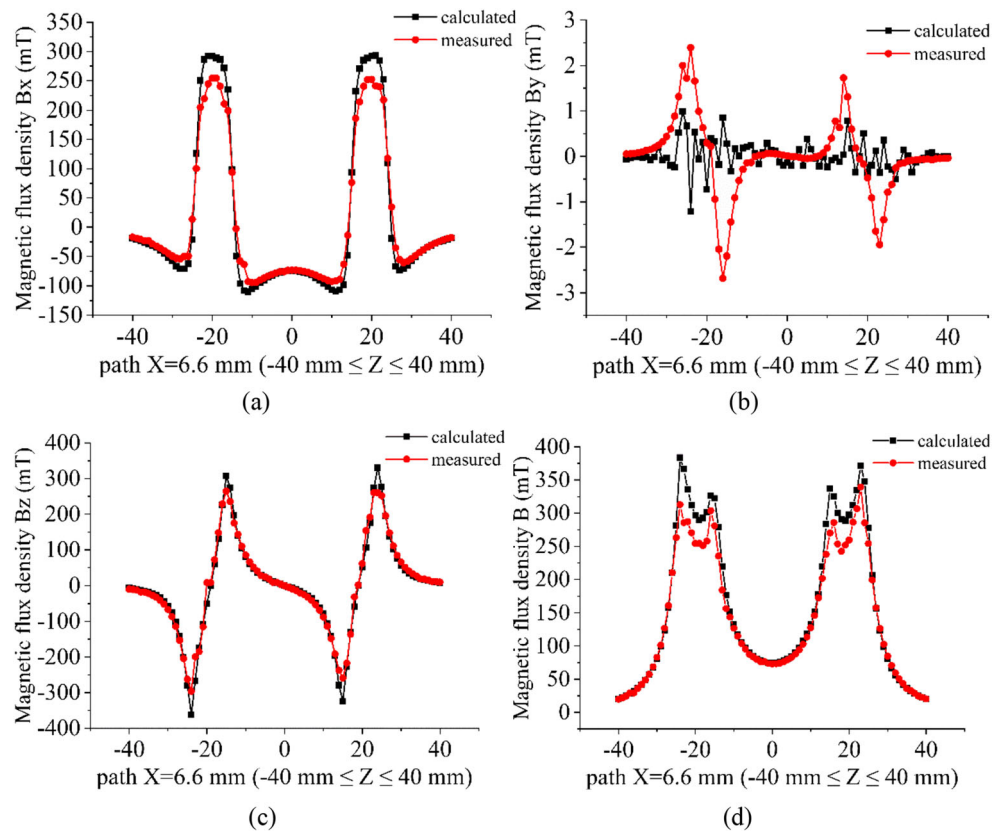
According to the calculated and measured results in Fig. 8, it can be seen that there are clear differences between them. In order to improve the accuracy of calculation results, the parameters of the magnetic ring were changed. The correction method is to repeatedly correct the residual induction and coercive force parameters, and compare each calculated result with the measured result until the calculated value and the measured value are within a set error range. After multiple calculations, the final modified residual induction is 1.42 T, and the coercive force is 900 kA/m. Figure 9 illustrates the magnetic flux distribution on the same path ($-40 \text{ mm} \leq Z \leq 40 \text{ mm}$, $X = 6.6 \text{ mm}$, $Y = 0 \text{ mm}$) before and after modifying the parameters. Comparing the calculated value with the measured value, it can be found that the calculated value is closer to the measured value after the parameter was modified.

Figure 10 states the magnetic flux distribution on the path of different heights (hx) from the surface of the magnetic ring. It can be seen that the magnetic field decays rapidly on the surface of the magnetic ring, and the edge effect is only apparent near the surface of the magnetic ring. On a plane of 2 mm ($X = 7.6 \text{ mm}$) from the surface of the PM ring, the edge effect has become less apparent. On a plane of 40 mm ($X = 45.6 \text{ mm}$) from the surface of the magnetic ring, the magnetic field is almost close to zero.

4.2 Calculated and Measured Results of PM Rotor Magnetic Field

Using the method of calculating the magnetic flux density and distribution of the magnet can conveniently carry out the application design research of the magnet, and can save experiment cost and improve efficiency as well. Correcting the

Fig. 8 Comparison of the measured value with the calculated value on the path of magnetic ring surface, $-40 \text{ mm} \leq Z \leq 40 \text{ mm}$; $X = 6.6 \text{ mm}$; $Y = 0 \text{ mm}$. **a** B_x . **b** B_y . **c** B_z . **d** B



calculation parameters through the magnetic field measurement of the magnet can help with accuracy improvement of the calculation result.

The external magnetic flux distribution of the PM rotor was calculated by using the FEA method, the coercive force and residual induction are the corrected parameters, and the orientation direction of each pair of adjacent PM rings is reversed. Figure 11 declares the magnetic flux distribution results on the axial path ($-15 \text{ mm} \leq X \leq 85 \text{ mm}$) of 1 mm away from the outer surface of the PM rotor. The actual position of rotor is $0 \text{ mm} \leq X \leq 70 \text{ mm}$. The magnetic field measurement system designed in this paper was used to measure the magnetic field of the rotor on the same path. Figure 12 indicates the comparison of measured and calculated results of B_x , B_y (B_r), and vector sum B , the calculation results match the measured results well, once again verified the correctness and accuracy of the calculation method.

From the results of the spatial magnetic flux distribution shown in Fig. 11, the magnetic field (B_x) in the axial direction of the PM rotor has approximative cosine periodic distribution on the axial path of the rotor, and the magnetic field (B_y) in the radial direction has approximative sinusoidal periodic distribution on the axial path of the rotor. From the radial magnetic flux distribution at different axial positions shown in Fig. 13, the magnetic field of the outer surface of the PM rotor exhibits an exponential decreasing distribution in the radial direction,

and the magnetic flux density and the magnetic field gradient are the largest in the iron pole.

Since the PM rotor has a structural feature of periodically repeating the arrangement, a unit model as shown in Fig. 14 can be established to discuss which structural parameters cause changes in the magnetic field distribution. Where b is the axial thickness of the PM ring and w is the axial thickness of the iron ring, h is the radial thickness of PM ring and the iron ring, and g is the gap between the stator and rotor of the superconducting magnetic bearing.

Since the permanent magnet rotor is assembled on the shaft, the radial thickness h of the PM rotor will affect the diameter of the shaft and the dynamics of the rotor system. When the stator inner diameter, gap g , and design speed of a HTS magnetic bearing are given, the radial thickness h of the PM rotor can be determined. But the magnetic field of the PM rotor can be changed by the structural parameters b and w in different forms. According to the application requirements of the actual HTS magnetic bearing in the axial and radial bearing capacity, the structural parameters b and w of the PM rotor need to be rationally designed to change the magnetic flux distribution of the rotor magnetic flux in the axial and radial directions; thus, corresponding force and stiffness HTS magnetic bearing requirements can be obtained in the axial and radial directions. The finite element calculation method used in this paper can easily calculate the magnetic field of the PM

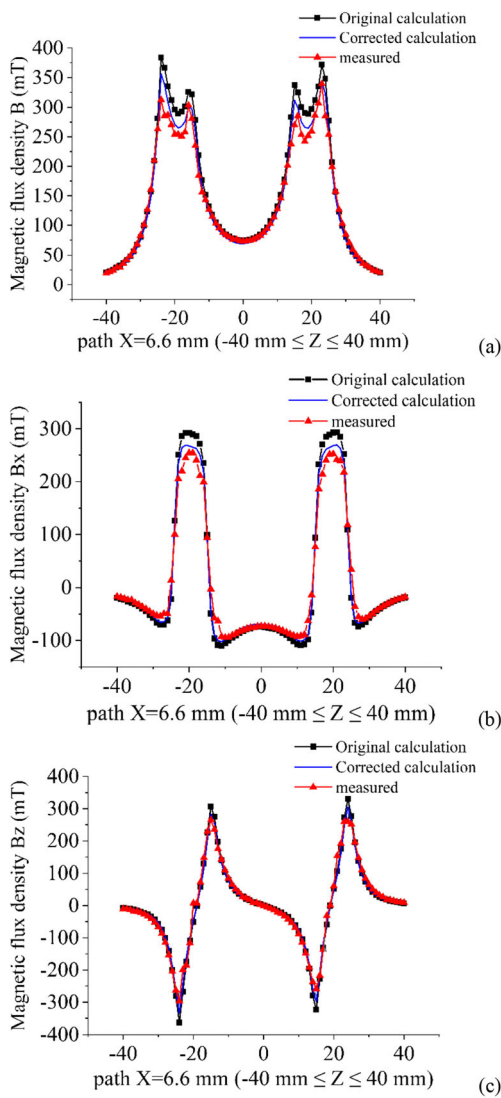


Fig. 9 Comparison of calculated value and measured value before and after modifying the parameters. **a** B . **b** B_x . **c** B_z

rotor, which is helpful to promote the structural design of the HTS magnetic bearing rotor.

4.3 Magnetic Ring Magnetic Field Uniformity Measurement

For a high-speed rotating machine using HTS magnetic bearings, the magnetic field uniformity of the magnets will affect the circumference magnetic field of the PM rotor, which has a particularly significant impact on its dynamic stability. However, there are differences in the magnetization effect of a single permanent magnet in actual production, and there are also differences between the permanent magnets even from the same batch. This will lead to poor magnetic field uniformity outside the PM rotor and affect the bearing performance of the bearing system. Based on the magnetic field measurement system in this paper, the PM rings applied in batch were

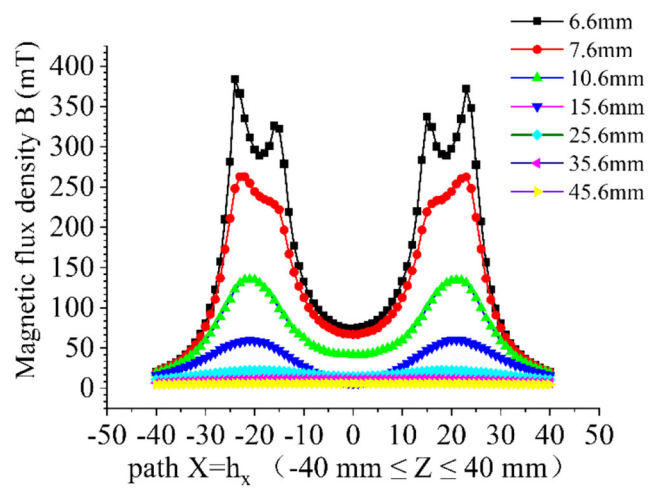


Fig. 10 Magnetic flux distribution on the path of different heights

measured and screened. The purpose is to select magnetic rings with uniform and consistent magnetic field to form a PM rotor and improve the stability of the HTS magnetic bearing.

In order to ensure that the measurement conditions for each magnetic ring were the same, before measuring the uniformity of the ring, the concentricity of the magnetic ring holder and the rotating moving mechanism should be adjusted, then the magnetic ring holder should be fixed. The relative position of the measurement probe and the magnetic ring should be adjusted, and the probe position should be unchanged for each measurement, too. In the measurement, the sample stage is 0 controlled to rotate for 360° . Since the iron ring design of the PM rotor can homogenize the magnetic field to a certain extent [14], thus, in order to improve the screening efficiency, the magnetic field was measured at 45 degrees per interval on the circumference of the ring. Figure 15 explains the measurement results of four magnetic rings randomly selected from

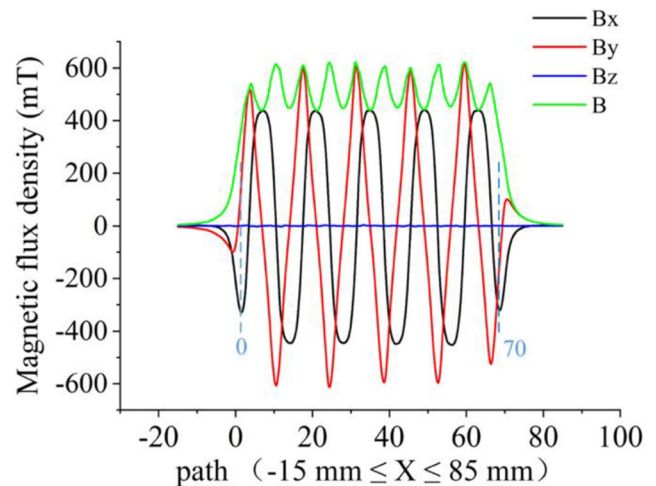


Fig. 11 Calculation results of magnetic flux distribution on the surface of PM rotor

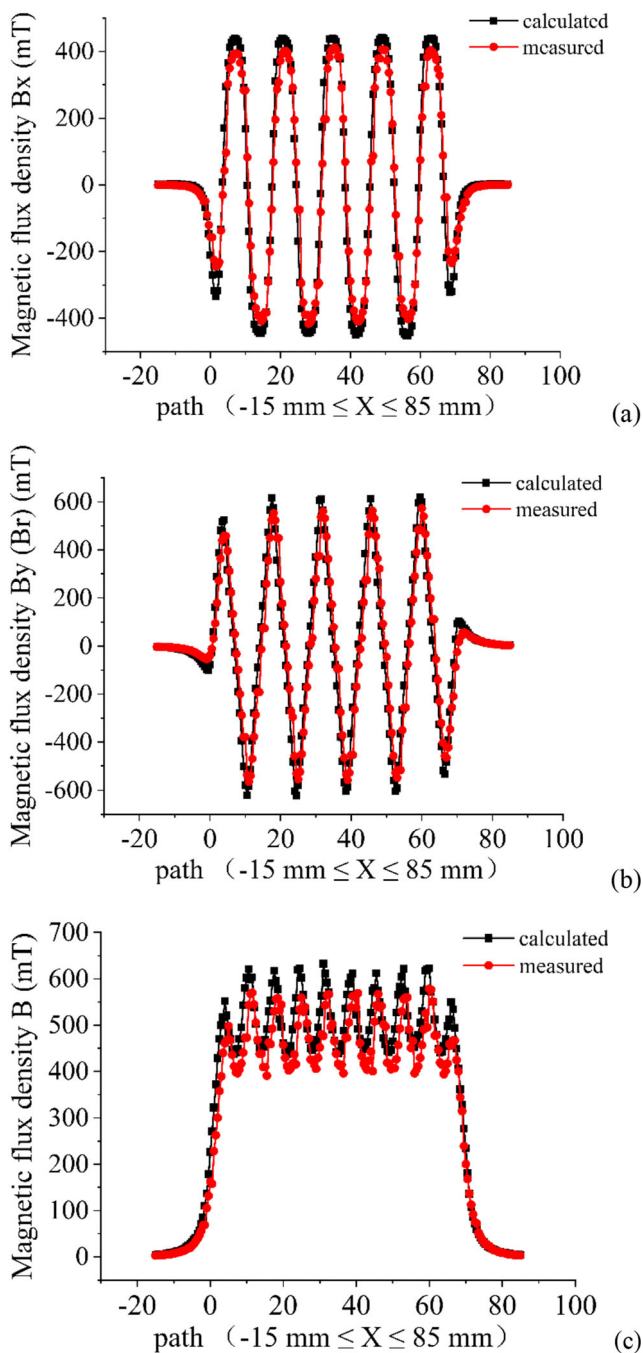


Fig. 12 Comparison of calculated rotor magnetic field with measured. a B_x . b B_y (B_r). c B

the batch of magnetic rings. By dividing the difference between the maximum value and the minimum value basing on average value, the uniformity of the magnetic rings on the circumference can be obtained. It can be found that the uniformity of different magnetic rings on the circumference has big differences. Therefore, by measuring the magnetic field of the magnetic ring, the magnetic ring within a certain uniformity requirement can be selected.

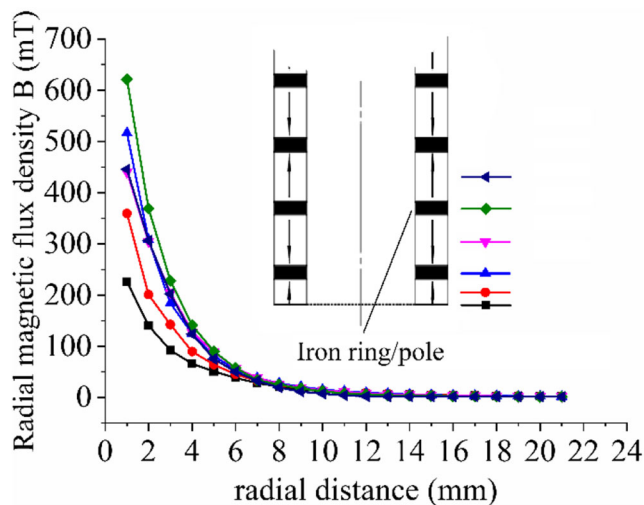


Fig. 13 Radial magnetic flux distribution of the rotor at different axial positions

4.4 Low Temperature Performance Measurement of $Nd_2Fe_{14}B$ Magnetic Ring

For the HTS magnetic bearing used in the liquid nitrogen temperature (77 K), the magnetic field performance of the PM ring at liquid nitrogen temperature directly affects the HTS bearing performance. In this study, the magnetic field measurement system and the one-dimensional cryogenic probe were used to experimentally study the performance of the PM ring at liquid nitrogen temperature. The position of the probe was fixed during the experiment to ensure that each measurement process was performed under the same conditions. Figure 16 shows the magnetic field performance measurement results of four magnetic rings randomly selected from the batch of $Nd_2Fe_{14}B$ (N52) magnetic rings at liquid nitrogen temperature. From the magnetic rings 1 to 4, the performance of the magnetic rings at the liquid nitrogen temperature (77 K) is increased by 8.86%, 9.5%, 8.7%,

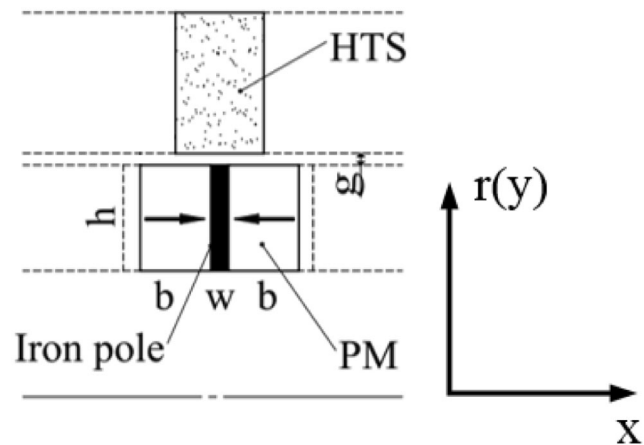


Fig. 14 PM rotor unit model

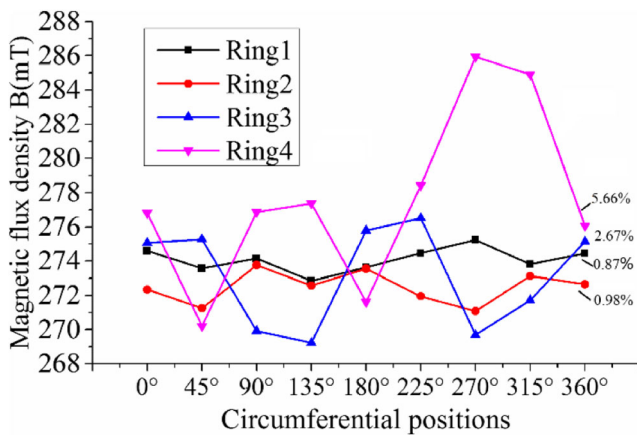


Fig. 15 Magnetic ring uniformity measurement

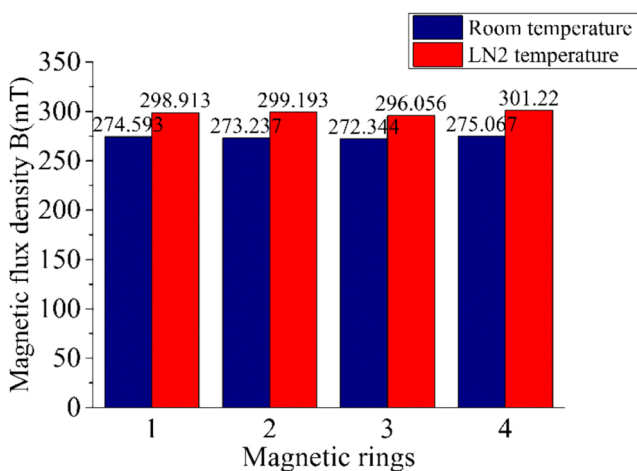


Fig. 16 Magnetic ring performance test results at LN2 temperature

and 9.5% relative to the magnetic ring performance at room temperature (295 K).

The measurement results show that the liquid nitrogen temperature is beneficial to the performance improvement of the permanent magnets. At the same time, the magnetic field performance measurement of the PM ring after immersion in liquid nitrogen and rewarming (repeated no less than 10 times) was carried out in this study, and the results indicate that the magnetic field of the magnetic ring remains unchanged. As a result, the performance of the HTS magnetic bearing will be further improved when it is applied at liquid nitrogen temperature (77 K).

5 Conclusion

This paper calculated the magnetic flux density and distribution of permanent magnets by using ANSYS finite element analysis method. A magnetic field measurement system which

can measure the magnetic field at room temperature (295 K) and liquid nitrogen temperature (77 K) was designed and constructed. The comparison of the calculated results with the measured results proved the correctness and accuracy of the finite element analysis method. Based on the calculation method and magnetic field measurement system, the main conclusions obtained in this paper are as follows:

1. The magnetic flux distribution on the path of different heights from the surface of the PM ring is obtained, and the magnetic field decays rapidly on the surface of the magnetic ring.
2. The axial and radial magnetic flux distribution of the PM rotor is obtained and analyzed, and the finite element calculation method used in this paper can easily calculate the magnetic field of the PM rotor, which is helpful to promote the structural design of the HTS magnetic bearing rotor.
3. The uniformity of the magnetic rings on the circumference was measured by the magnetic field measurement system, which can be used to measure and select the magnetic rings with uniform and consistent magnetic field to improve the stability of the HTS magnetic bearing.
4. The magnetic field performance of the Nd₂Fe₁₄B magnets N52 at liquid nitrogen temperature is increased by about 9% relative to the performance at room temperature (295 K) is obtained. It can be predicted that the application of the PM rotor at liquid nitrogen temperature will be beneficial to the performance improvement of the HTS magnetic bearing.

Funding Information This work is financially supported by the fund of the State Key Laboratory of Technologies in Space Cryogenic Propellants, SKLTSCP1902, and the fund of National Research and Development Project for Key Scientific Instruments, ZDYZ2014-1.

References

1. Caplanne, G., Berthier, R., Pfister, R., Ronayette, L., Pissard, M., Vincent, B., et al.: Cryogenic system for the 43 T hybrid magnet at LNCMI Grenoble: from the needs to the commissioning. *IOP Conf. Ser. Mater. Sci. Eng.* **171**, 012107 (2017). <https://doi.org/10.1088/1757-899x/171/1/012107>
2. Bevins, B.S., Chronis, W.C., Keesee, M.S.: Automatic Pumpdown of the 2K Cold Compressors for the CEBAF Central Helium Liquefier. *Adv. Cryog. Eng.* **41**, 663–668 (2011). https://doi.org/10.1007/978-1-4613-0373-2_86
3. Lee, K., Kim, B., Ko, J., Jeong, S., Lee, S.S.: Advanced design and experiment of a small-sized flywheel energy storage system using a high-temperature superconductor bearing. *Supercond. Sci. Technol.* **20**, 634–639 (2007). <https://doi.org/10.1088/0953-2048/20/7/009>
4. Ichihara, T., Matsunaga, K., Kita, M., Hirabayashi, I., Isono, M., Hirose, M., et al.: Application of superconducting magnetic bearings to a 10 kWh-class flywheel energy storage system. *IEEE Trans. Appl. Supercond.* **15**, 2245–2248 (2005). <https://doi.org/10.1109/TASC.2005.849622>

5. Ma, K.B., Postrekhin, Y.V., Chu, W.K.: Superconductor and magnet levitation devices. *Rev. Sci. Instrum.* **74**, 4989–5017 (2003). <https://doi.org/10.1063/1.1622973>
6. Navau, C., Del-Valle, N., Sanchez, A.: Macroscopic modeling of magnetization and levitation of hard type-II superconductors: the critical-state model. *IEEE Trans. Appl. Supercond.* **23**, 8201023–8201023 (2013). <https://doi.org/10.1109/TASC.2012.2232916>
7. Matsuura, Y.: Recent development of Nd–Fe–B sintered magnets and their applications. *J. Magn. Magn. Mater.* **303**, 344–347 (2006). <https://doi.org/10.1016/j.jmmm.2006.01.171>
8. Hu: Bo-ping, status and development tendency of rare-earth permanent magnet materials. *J. Magn. Mater. Devices.* **45**, 66–77 (2014). <https://doi.org/10.3969/j.issn.1001-3830.2014.02.016>
9. Fidler, J., Schrefl, T., Hoefinger, S.: Current status and recent topics of rare-earth permanent magnets. *J. Phys. D: Appl. Phys.* **44**, 1–11 (2011). <https://doi.org/10.1088/0022-3727/44/6/064001>
10. Wen-Yan, H.: Property and research progress of NbFeB permanent magnets. *Mod. Electron. Tech.* **35**, 151–152 (2012). <https://doi.org/10.16652/j.issn.1004-373x.2012.02.016>
11. El-refaie, A.M., Alexander, J.P.: Rotor End Losses in multi-phase fractional-slot concentrated- winding permanent magnet synchronous machines. *Ind. Appl. IEEE Trans.* **47**, 2066–2074 (2010). <https://doi.org/10.1109/TIA.2011.2162049>
12. Werfel, F.N., Flögel-Delor, U., Rothfeld, R., et al.: HTS magnetic bearings. *Phys. C Supercond. Appl.* **376**, 1482–1486 (2002). [https://doi.org/10.1016/S0921-4534\(02\)01054-7](https://doi.org/10.1016/S0921-4534(02)01054-7)
13. Werfel, F.N., Floegel-Delor, U., Riedel, T., et al.: Progress toward 500 kg HTS bearings. *IEEE Trans. Appl. Supercond.* **13**(2), 2173–2178 (2003). <https://doi.org/10.1109/TASC.2003.813027>
14. Werfel, F.N., Floegel-Delor, U., Rothfeld, R., Goebel, B., Wippich, D., Riedel, T.: Modelling and construction of a compact 500 kg HTS magnetic bearing. *Supercond. Sci. Technol.* **18**, S19–S23 (2005). <https://doi.org/10.1088/0953-2048/18/2/005>

Publisher's Note Springer Nature remains neutral with regard to jurisdictional claims in published maps and institutional affiliations.